Superhydrophobicity of polymer films via fluorine atoms covalent attachment and surface nano-texturing

Jinlong Zha, Sahal Saad Ali, Jérémy Peyroux, Nicolas Batisse, Daniel Claves, Marc Dubois, Alexander P. Kharitonov, Guillaume Monier, Thierry Darmanin, Frédéric Guittard, et al.

Superhydrophobicity of polymer films via fluorine atoms covalent attachment and surface nano-texturing

Jinlong Zha[1], Sahal Saad Ala[1], Jérémy Peyroux[1], Nicolas Batisse[1], Daniel Claves[1], Marc Dubois[1,], Alexander P. Kharitonov[2,#], Guillaume Monier[4,5], Thierry Darmanin[6], Frédéric Guittard[6], Leonid N. Alekseiko[7]*

[1] Institut de Chimie de Clermont-Ferrand (ICCF), Université Blaise Pascal, UMR CNRS 6296, 63177 Aubiere, Cedex, France

[2] Branch of the Talrose Institute for Energy Problems of Chemical Physics of the Russian Academy of Sciences, Chernogolovka, Moscow region, 142432, Russia.

[3]Tambov State Technical University, Sovetskaya street, 106, Tambov, 392000, Russia.

[4] Clermont Université, Université Blaise Pascal, Institut Pascal, BP 10448, F-63000 Clermont-Ferrand, France

[5] CNRS, UMR 6602, IP, F-63171 Aubière, France

[6] Univ. Nice Sophia Antipolis, CNRS, Laboratoire de Physique de la Matière Condensée (LPMC), UMR 7336, Parc Valrose, 06100 Nice, France

[7]Far Eastern Federal University, 8 Sukhanova Str., 690950 Vladivostok, Russia

***Corresponding AuthorTel:** +33 4 73 40 71 05. **E-mail:** marc.dubois@univ-bpclermont.fr (M. Dubois)

[#] in memory of Prof. Alexander Kharitonov

Abstract

Surface micro/nano-texturing combined with the presence of fluorine atoms can result in superhydrophobicity. Different strategies are investigated in order to determine the critical parameters to reach such properties. On the one hand, fluorine atoms were grafted by direct fluorination of carbon nanofibers (treatment with gaseous F_2 resulted in samples denoted F-CNF), and on the other hand, fluorinated polymers such as polyvinylidene fluoride PDVF or poly(ethylene oxide) POE fluorinated with F_2 as well as commercial hydrophobic polymers like polystyrene (PS) are used as binders and/or polymer matrix to produce nanocomposites. Stable superhydrophobic properties are obtained with F-CNF/PVDF nanocomposites micro-textured with femtosecond laser ablation and F-CNF/PS nanocomposites, with water contact angles of 157° and 155° respectively. Polystyrene was also covalently grafted onto the nanofiber surface through a two-step process: fluorination followed by monomer grafting. The polymerization of styrene ensures both covalent grafting onto the carbonaceous surface and a good dispersion of nanofibers inside the polymer lattice. Moreover, C-F bonds exhibit a covalent nature in fluorinated nanofibers, in PVDF, in fluorinated POE and in the fluorinated resin and ensure an improved chemical stability for studied nanocomposites and micro-textured resin. Comparison of the water contact angles for nanocomposites with PS, PVDF, POE and fluorinated POE highlights that the polymer matrix imposes its surface chemistry whereas the emergence of nanofibers results in a necessary nano-texturing.

Keywrods: Fluorination ; composite; Polymer ; micro-texturing ; nanofibers ; nanotubes ; superhydrophobicity ; laser ablation

1 INTRODUCTION

Superhydrophobic films can be used for many potential applications in optics domains [1], self-cleaning windows, roof tiles, textiles, solar panels and applications requiring anti-biofouling, drag reduction in fluids (micro/nanochannels) [2] and metal corrosion resistance [3-5], for example. The surface morphology, namely the roughening, plays a key role for superhydrophobicity. Two cases may be described: either solid-liquid interface [6], or when air is trapped on a rough interface between the surface and the liquid droplet [7]. For the second case, surface hydrophobicity is enhanced because air is considered as an absolute hydrophobic material (contact angle of 180°) [8,9] and because the trapped air reduces the adhesion of the water droplet. Hierarchical surface micro- and nanostructuring are then very efficient to reach superhydrophobicity. Examples from nature underline well this assumption: the unique hierarchical surface structure of the Lotus leaf consisting of papillae, wax clusters and wax tubules makes it an outstanding model. Shark skin is covered by very small individual tooth-like scales called dermal denticles [10]. The water strider legs are covered by large numbers of oriented tiny hairs (microsetae) with fine nanogrooves. The air trapped in spaces between the microsetae and nanogrooves leads to the superhydrophobicity property of the legs, with a contact angle around 167° [11]. Fluorine chemistry was often used to reach superhydrophobicity. Fluoroalkylsilane molecules were often used as fluorine source when added by a simple reaction of the silane groups on coatings [12-16], on acid edged surface [17], on carbon nanotubes deposited onto polystyrene (PS) colloidal crystals [18], on nanofibrils [19] or on monodisperse silica nanoparticles [20]; Using chemical vapor deposition, fluoroalkylsilane was also grafted onto a electrodeposited poly(3,4-ethylenedioxythiophene) (PEDOT) film to prepare conductive superhydrophobic coating [21].

Substitution compound of hydrogen atom of hydrocarbon by fluorine atom decreases its surface energy because of the strong covalence and small polarizability of the C-F bond. A typical hydrophobic material is polytetrafluoroethylene (Teflon). The surface energy of material depends on the character of terminal group of the material, and decreases in order $-CH2 \rightarrow -CH \rightarrow -CF \rightarrow -CF_3$ and, the critical surface tension of $-CF_3$ is 67 dyn/cm. The surface energy of solid surface is proportional to the surface fluorine atomic ratio [22]. Nevertheless, the presence of fluorinated groups (CF, CF_2 and CF_3) on the surface and the subsequent surface energy decrease are not enough to reach superhydrophobicity. As a matter of fact, flat surfaces with $–CF_3$ terminated groups, having the lowest free energy, exhibit a maximum contact angle of only 120° [23]. Techniques similar to micro- and nanostructure fabrication, such as lithography, etching, deposition and self-assembly were used to fabricate superhydrophobic surfaces; The aim was to create the desired roughness. Nevertheless, fluorinated materials have a limited solubility which makes it difficult to tailor their surface structure afterwards. However, they may be linked or blended with other materials, which are often easier to roughen, in order to make superhydrophobic surfaces, e.g. using CF_4/O_2 plasma etching of polydimethylmethylsiloxane/polytetrafluorethylene (PDMS/PTFE) composite [24]; 1,1,-2,2,tetrahydroperfluorodec-trichlorosilane (PF3) or perfluorodecyltriethoxysilane (PFDTES) self-assembled monolayer (SAM) deposited on micro-patterned substrates, silicon [25] or poly(methyl methacrylate) (PMMA) [26], respectively, resulted in superhydrophobicity. An alternative way is the fluorination of polymer films. The fluorination and the decomposition into CF_4 and C_2F_6 species compete and the surface roughness is increased. A superhydrophobic slippery surface onto PS, low density polyethylene (LDPE) or PDMS substrates were achieved by CF_4 plasma etching resulting in a simultaneous roughening and fluorinating action [27-30]. Plasma

etching was also carried out on two-dimensional hexagonally ordered honeycomb arrays [31]. An oxyfluorination followed by a graft polymerization double-step process was used to modify the LDPE surface properties [32]. Coatings prepared with raspberry-like polymer particles fluorinated by reaction with an excess of a statistical copolymer poly(2-(perfluorooctyl)ethyl methacrylate-co-glycidylmethacrylate), P(FOEMA-co-GMA) exhibited superamphiphobic properties [33]. Electrically conductive superhydrophobic coatings were also prepared by electrochemical polymerization methods with fluorinated monomers [34-37]. Fluorinated polymer films have also been the starting material for treatments. Shiu et al. [38] reported PTFE film treatment with oxygen plasma resulting in a superhydrophobic surface with a contact angle of 168°. PTFE substrates plasma chemical roughening followed by a deposition of low surface energy plasma polymer layers has been also successful [39]. Hierarchical nanostructures were also created on PTFE nanocones [40]. A contact angle of water on the surface of a new composite, which are made of highly fluorinated polymer and nickel was over 170° (for example Nickel plating 67°, Teflon 110°) [41] .

On the other hand, covalent grafting of fluorine atoms onto different carbonaceous materials was investigated for the aim of superhydrophobicity, e.g. well dispersed fluoro-containing copolymer onto the carbon fabric [42], MWCNTs dispersed in fluoropolymer films [43], carbon nanotubes fluorinated by laser plasma-type [44], carbon black surface covalently grafted with of perfluorocarbon and perfluoropolyether chains [45] and ordered mesoporous carbon materials treated with fluoroalkylsilane [46]. In every case, both surface chemistry and roughness influence the superhydrophobic properties.

Among the fluorination methods described in the literature, to the best of our knowledge, the direct fluorination was never reported. It consists in a gas/solid reaction using several fluorinating agents, molecular fluorine F_2 and solid fluorinating agent that releases atomic fluorine $F^{\bullet}$ by thermal decomposition [47-48]. In the present paper, the direct fluorination was applied to both polymer and carbonaceous nanomaterials, namely carbon nanofibers, in order to prepare superhydrophobic surfaces.

2 EXPERIMENTAL SECTION

2.1. Materials and methods

Three routes were investigated (Figure 1):

- **ROUTE 1.** The direct fluorination of micro-textured polymer resin, i.e. micrometric cylindrical plots of 15 µm in diameter and separated by 40 µm distance, was considered. The micro-texturing of the resin was performed using photosensitive resin (SU-8 epoxy-based negative photoresist) and well-designed masks by a conventional photolithography process. This micro-texturing must be partly preserved after fluorination although the high reactivity of the polymer resin with the fluorinated agent. Xenon difluoride XeF_2 has been chosen as the fluorinating agent instead of molecular fluorine F_2. This way allows a better control of the fluorination, and even diffusion in the bulk, whereas process with F_2 is rather a surface treatment.
- **ROUTE 2.** Fluorinated nanofibers were included in films with poly(vinylidene fluoride) (PVDF) as a binder. The fluorinated nanofibers could provide both the fluorinated surface and the adequate nano-roughness because of their diameter, with an average value of 140 nm. Additional micro-texturing will be added by femtosecond laser ablation.
- **ROUTE 3.** Such way has been recently published [48] and is discussed in the present paper for comparison. Hydrophobic polystyrene (PS) was grafted on the same fluorinated nanofibers via a two-step process: fluorination of

the fibers followed by a gaseous styrene monomers grafting. Dangling bonds (radicals) formed on nanofiber surface during the fluorination act both as grafting sites and initiators of the styrene graft polymerization. PS/fluorinated nanofibers nanocomposites were then obtained. Films fabricated from that nanocomposite were prepared by evaporation of the grafted nanofibers dispersion in toluene.

The first route has used the direct fluorination of a micro-textured resin whereas the two others routes have taken the benefit of the fillers (carbon nanofibers) fluorination.

2.1.1. Route 1

Commercial resin SU-8 2025 (Microchem) is a high contrast, epoxy based photoresistant resin designed for micromachining and other microelectronic applications, where a thick, chemically and thermally stable image is desired. It has been designed as a permanent, highly cross-linked epoxy material and it is extremely difficult to dissolve it in conventional solvents.

Fluorination using XeF_2

The resin surface fluorination was carried out with xenon difluoride (XeF_2). It is solid and its reactivity relies on its vapour pressure which is equal to 3.8 mm Hg at 25 °C and 318 mm Hg at 100°C [47].

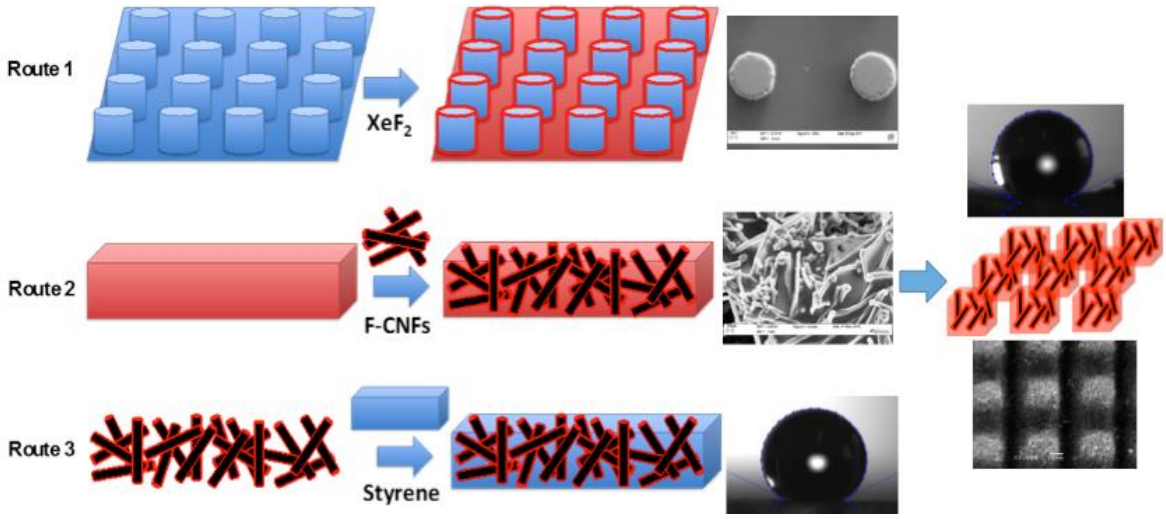

Figure 1. Direct fluorination to achieve superhydrophobicity. Red color marks the presence of fluorine atoms on the resin surface (Route 1), in PVDF and nanofibers (Route 2) and in nanofibers (Route 3).

XeF_2 was decomposed onto the resin surface according to the following equation: $XeF_2 \rightarrow Xe + 2F^{\bullet}$. It is to note that the reaction also occurred onto the silicon substrate. This side reaction was beneficial because it avoided severe decomposition of the resin. XeF_2 was home made using the reaction of Xe with F_2 at 300°C; XeF_2 crystals were collected on a cold finger inside the reactor. Micro-textured resins on a silicon wafer were placed in a stainless container with a gas-tight cover. XeF_2 was placed in a smaller

alumina crucible in order to avoid direct contact with the film. Finally, the stainless container was tightly closed and kept at 120°C for 12h.

2.1.2. Route 2

Fluorination of carbon nanofibers

High purity (>90%) carbon nanofibers, 2–20 microns in length, were supplied by the MER Corporation, Tucson, Arizona. They were obtained by chemical vapor deposition (CVD) and heat treated at 1800 °C in an argon atmosphere to enhance their graphitization degree.

Fluorination by gaseous F_2 was performed in a dedicated fluorinating apparatus: the compound to fluorinate was placed at the center of a tubular reactor. The latter is made of a nickel tubing passivated with NiF_2 and is gas-tight in order to prevent any fluorine leakage. The reactor was subsequently flushed with nitrogen gas and fluorine was introduced for 1h. After fluorination, the reactor was flushed with nitrogen to remove unreacted fluorine traces. Fluorinated carbon nanofibers were synthesized by the direct fluorination using a static method. In this case, pure fluorine gas was used in a closed reactor. The initial pressure was equal to 1 atm. Static method allowed the increase of the reaction yield and the fluorination of a large amount of fibers. The fluorination was performed at 450 °C with 100 g of fibers during 6h. The resulting sample is denoted as F-CNF.

Fluorinated nanofibers fluorination level 'x' in CFx composition, i.e. the F/C atomic ratio, was determined both by gravimetric measurements upon fluorination (weight uptake) and by quantitative ^{19}F NMR measurements. In this study the F/C atomic ratio of the fluorinated CNF was equal to 0.8.

Preparation of F-CNF/PVDF nanocomposite film

F-CNF was mixed in acetone with polyvinylidene Fluoride (PVDF), which was supplied by Arkema. The F-CNF weight percentage was equal to 40 wt. %. The F-CNF/PVDF/acetone mixture was sonicated for 2 h. The dispersion was then deposited onto a glass substrate and acetone was evaporated (drop casting). Dip coating was also used with the same dispersion.

Microstructuration by femtosecond laser ablation

The as-prepared F-CNF/PVDF composites films were microstructured by laser ablation using a NEWPORT µFab laser micromachining workstation coupled with a EKSPLA FF3000 femtosecond laser (1030nm, 250fs). The laser beam was focused by an Olympus objective (NA 0.25) to give a spot size of 5µm approximately. The fluence was set to 0.5 J cm^{-2} at a repetition rate of 2 MHz and the displacement speed has been fixed at 800 µm s^{-1}.

2.1.3. Route 3

This work was fully described in a recent paper [50].

2.2. Characterization

FTIR spectra (recorded either with ATR mode -diamond crystal and DTGS TEC detector - or with pressed KBr pellets in absorbance mode) were measured with Nicolet 5700 FTIR spectrometer. All the spectra were measured at 4 cm^{-1} resolution and 512 scans were taken for each spectrum.

Multinuclear NMR measurements were performed using BRUCKER AVANCE spectrometer, with working frequencies for ^{13}C, ^{1}H and ^{19}F of 73.4, 300.1 and 282.2 MHz, respectively. A magic angle spinning (MAS) probe (Bruker) operating with a 4 mm

rotor was used. For MAS spectra, a simple sequence was performed with a single π/2 pulse length of 3.5, 4 and 3.5 µs for ^{1}H, ^{19}F and ^{13}C, respectively. A cross polarization/MAS NMR probe (Bruker) with proton decoupling on a 4 mm rotor was used. ^{1}H and ^{13}C chemical shifts were externally referenced to tetramethylsilane (TMS). ^{19}F chemical shifts were referenced with respect to $CFCl_3$.

The X-ray photoelectron spectra (XPS) were recorded in an UHV chamber equipped with a hemispherical analyzer OMICRON EA125 and a dual anode Al–Mg X-ray source operating at 240 W under a residual pressure of 1×10^{-8} Pa. Mg Kα source (1253.6 eV) at an incident angle of 55° and a normal detection were used for analysis. The spectrometer pass energy was set to 50 eV for survey spectrum and to 20 eV for core peak records. All the binding energies were referenced to the C-C bonds in C1s peak at 285.0 eV. The treatment of core peaks was carried out using a nonlinear Shirley-type background [49]. A weighted least-square fitting method using Voigt function was applied to optimize the peak positions and areas. The surface composition quantification was based on Scofield's relative sensitivity factors [52] and inelastic mean free pass were calculated from TPP2M method [53] considering the analyzed depth homogeneous composition.

Morphology and surface composition of samples were also investigated by Scanning Electron Microscopy (SEM). The electron beam energy was fixed to 3.00 keV and working distance was over 4-6 mm range.

Static contact angle measurements were recorded by an Attension Theta Lite Optical Tensiometer equipped with an imaging source camera. All contact angles were the averaged values of measurements performed on five different locations on the sample surface.

3. RESULTS AND DISCUSSION

3.1. Route 1

The SEM images of raw and treated samples with XeF_2 micro-textured resins are shown in the Figure 2. The cylindrical geometry of the plots was not changed after the fluorination in mild condition. Gaseous XeF_2 decomposition onto either the resin surface or Si substrate released a defined amount of atomic fluorine which reacted with the resin and with the Si substrate to form gaseous SiF_4. Such a side reaction allowed milder conditions to be applied for the resin. Nevertheless, the plots cylindrical tops seemed cut down by the fluorination and appeared less angular. Neither cracks nor holes were observed on the resin surface after the fluorination, implying the mild attachment of fluorine atoms. In order to evidence the fluorine atom covalent attachment to the polymer surface, XPS was performed on the fluorinated micro-textured resins and also on 25 µm-thick flat resin film. Three additions of XeF_2 were carried out in order to progressively increase the fluorine content. Fluorinated polymer surface composition and the CH_n/CHF and CHF/CF_2 ratios have been derived from the XPS peaks considering analyzed depth homogeneous composition (this approximation did not take into account the adventitious species coming from air exposure but allowed to obtain the relative evolution of the surface composition with the fluorination process). Fig. 3 shows the micro-textured resin F1s and C1s core peaks before and after the fluorination. Tables 1 and 2 summarize the atomic content and the assignments of C1s spectra respectively. The sample surface was oxidized and oxygen content depended on the fluorination conditions. The pristine polymer contained 20.3% oxygen atoms and a O/C atomic ratio was measured at 0.255. The first XeF_2 addition induced an O/C ratio increase to 0.527, but further additions resulted in a O/C ratio decrease to 0.488 and 0.442. Fluorination always resulted in some C-C and C-H bond cleavages and radical (dangling bonds) formation which reacted with oxygen during the sample re-exposure to air. Oxygenated groups were then formed and the O/C ratio was increased. Two

components have been identified in the O1s: the first one located at 532.5 eV was assigned to C=O environments and another at 533.8 eV was attributed to oxygen atoms in C-O-C environment. For all the samples, nitrogen atoms were detected with an amount over 2.2-5.1% range.

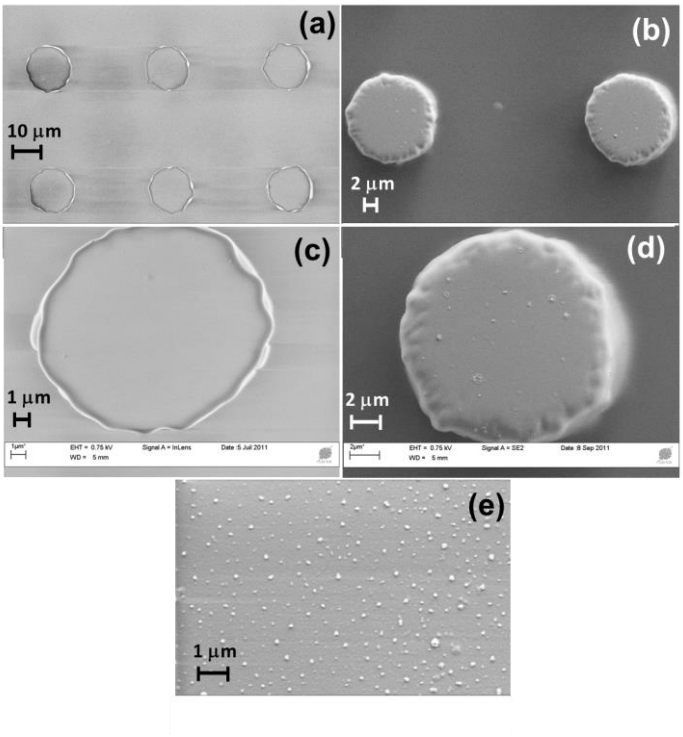

Figure 2. SEM images of raw (a, c) and fluorinated (b, d) micro-textured resins using adequate XeF_2 amount as a fluorinated agent. The fluorinated non-textured resin surface is presented for comparison (e).

XeF_2 successive additions resulted in a fluorine content increase (Table 1). Indeed, F/C ratio was increased from 0 to 0.612 (the intermediate values are 0.242 and 0.307). The O/C and F/C ratios for micro-textured resins were equal to 0.474 and 0.498 respectively. Thus the composition determined for the micro-textured resins was very close to the composition of the highly fluorinated resin which was treated under the same conditions.

Table 1. XPS analyses of fluorinated samples.

Samples	%C	%N	%O	%F	O/C X 100	F/C X 100	CH_n/CHF	CHF/CF_2
Pristine resin	79.7	0	20.3	0	25.5	0	-	-
Addition 1	55.3	2.2	29.1	13.4	52.7	24.2	2.30	-
Addition 2	52.9	5.1	25.8	16.2	48.8	30.7	1.95	-
Addition 3	47.4	2.9	21.0	29.0	44.2	61.2	1.40	3.19

Micro-textured resin	49.5	2.3	23.5	24.7	47.4	49.8	1.43	3.84

Table 2. The XPS C1s components assignment.

Chemical bond	**Shift *(eV)* Relative to the CH_n component at 285.0 eV**
$\underline{C}H_n$	-
$\underline{C}H_2$-CHF / $\underline{C}$-O	1.4
$\underline{C}H_2$-CF_2 / $\underline{C}$=O	2.5
$\underline{C}$HF-CH_2	3.7
$\underline{C}$HF-CF_2 / $\underline{C}$HF-CHF	5.0
$\underline{C}F_2$-CH_2 CF_x-$\underline{C}$F-$CF_{x'}$ (x,x'=2,3)	6.0
$\underline{C}F_2$-CHF / $\underline{C}F_2$-CF_2	7.0

F1s spectra of fluorinated samples confirmed the covalent nature of C-F bonds (Fig. 3c). Indeed, only covalent C-F bonds were observed in all the fluorinated sample spectra. F1s component binding energy (686.8 eV) observed in the case of all the fluorinated samples was attributed to a covalent F-C bond in a hydrocarbon environment [62]. The F1s component was very slightly shifted to a higher binding energy (+ 0.5 eV) according to the fluorine high content on the surface. Pristine and fluorinated resin C1s core peaks exhibited five to seven different components depending on the fluorination route. In agreement with literature data [54-56] , Table 2 reviews C1s components specific assignment. The C1s core peak in Figure 3a was well characterized for commercial polymers such as polyethylene with a major component located at 285.0 eV attributed to the polymer carbon and oxygen contaminations which are always present at the polymer surface (286.7 eV). As it was evidenced by C1s core peak deconvolutions, the fluorination route strongly influenced the carbon environment. Indeed, after XeF_2 addition, C-F bonds in CHF-CH_2 and CHF-CHF were detected at 288.7 eV and 290.0 eV. The CH_n/CHF ratios were equal to 2.30 and 1.95 for the addition 1 and 2 respectively. Further XeF_2 addition resulted in CF_2 group creation detected at 291.0 eV (CF_2-CH_2) and 292.0 eV (CF_2-CF_2) in the C1s spectra and a CF_2/CH_2 ratio of 3.19 was obtained. At the same time, the CH_n/CHF ratio decreased again to a value of 1.40 indicating again the increasing fluorination. In this case, the fluorination content (29.0 at.%) was the highest one. The XPS analysis of the micro-textured resin exhibited nearly the same results as the CH_n/CHF and the CF_2/CH_2 ratios were equal to 1.43 and 3.84 respectively. It is important to keep in mind that this analysis has been performed on the outmost surface layer which is thinner than 5 nm.

Thanks to mild fluorination conditions when XeF_2 was used, the resin micro-texturing was conserved and the surface became fluorinated. Covalent C-F bonds were evidenced by XPS. The water contact angles were measured on raw and fluorinated resin, flat and micro-textured.

For the flat non-structured resin film, spreading of the water droplet rapidly occurred; less than 30 s was necessary to reach a contact angle (called Young angle θc^{Y}) lower than 10°. Fluorination did not change this hydrophilic character regardless of the treatment conditions.

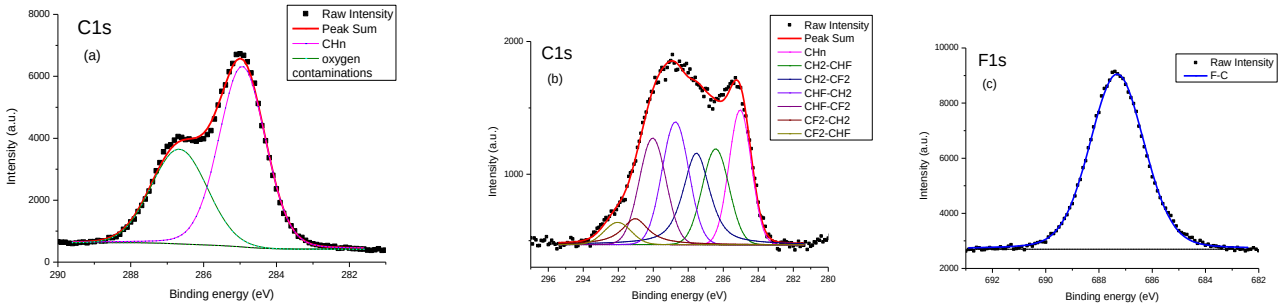

Figure 3. The micro-textured resin before (a) and after (b and c) fluorination XPS C1s and F1s spectra.

The micro-textured resin surface was also hydrophilic with nearly the same behaviour, but to the contrary after fluorination, the averaged contact angle θc was increased to 131±2 ° (6 recorded values). Thus the following two criteria must be filled to achieve highly hydrophilicity ($\theta c^{Y} < 10°$) into highly hydrophobicity ($\theta c = 131 \pm 2°$) conversion: (i) micro-texturing and (ii) fluorine atoms on the surface. In order to explain these results more appropriately, the Wenzel and Cassie-Baxter equation can be used to understand the effect of surface roughness. When the water droplets on the micro-textured surface are in the Wenzel state [6], all the surface roughness is completely wetted by water. The Wenzel equation is $\cos \theta c = r \cos \theta c^{Y}$, where r is a roughness parameter. The results obtained here cannot be explained with the Wenzel equation because it is possible to obtain extremely high θc but only if $\theta c^{Y} > 90°$. Only the Cassie-Baxter equation can predict extremely high θc regardless of the θc^{Y} value, which indicates the presence of air between the droplet and the surface [7]. The Cassie-Baxter equation is $\cos \theta c = r_f f \cos \theta c^{Y} + f - 1$. In this equation, r_f is the roughness ratio of the substrate wetted by the liquid, and f the solid fraction and (1 – f) the air fraction. This equation can lead to superhydrophobic properties if the air fraction is extremely important but also highly hydrophobic properties if the air fraction is less important. Here, our surfaces are “only” highly hydrophobic because θc^{Y} is extremely low ($\theta c^{Y} < 10°$) and also because the surfaces are micro-textured but not nano-textured.

Taking into account those promising results, the second route was investigated: fluorine atoms were provided both by the fillers and the polymer matrix. Fluorinated carbon nanofibers with $CF_{0.8}$ composition were used as fillers whereas PVDF acted as a binder.

3.2 Route 2

SEM images of the fluorinated CNF/PVDF film deposited on a glass substrate are shown in the Figure 4. Films with F-CNF weight percentages of 40 w.% were prepared by dip coating and drop casting and compared to the film fabricated from nude PVDF. The ^{19}F NMR spectrum of the nanocomposite is the superimposition of the spectra for PVDF and F-CNF without changes of their relative intensities and additional lines (Fig. SI1 in the supplementary information). No chemical changes and transfer of fluorine atoms occurred during the preparation of the nanocomposite.

SEM images (Fig. 4) of the F-CNF/PVDF nanocomposite film deposited by dip coating underlined interspersed fluorinated nanofibers homogeneous dispersion. Continuous PVDF matrix acted as a binder. Numerous fluorinated nanofibers emerged from the surface. Such a morphology increases the contact angle to 133 ± 2° in comparison with flat PVDF (110 ± 2°). In order to evaluate if the surface chemistry is imposed by the binder which totally covers the fillers or the fluorinated nanofibers, both binder and fillers were changed; poly(ethylene oxide), POE or $(CH_2CH_2O)_n$ (Aldrich), and non-fluorinated nanofibers were then used to prepare the composite film with the same method. In other terms, fluorine atoms are present neither on the polymer nor on the fillers. Except acetonitrile which replaced acetone for a better dispersion of POE, the operating conditions with dip coating were similar. The morphology appeared as very close to the one of F-CNF/PVDF with fibers that emerged from the polymer matrix (Fig. 4c and d). Nevertheless, the contact angle was of 80 ± 2° evidencing a hydrophilic character, which is imposed by POE (Table 3). The fluorination of the nanocomposite film was then carried at room temperature with 50 mbar of F_2 gas for 30 min. In such conditions, carbon nanofibers cannot be fluorinated; a temperature of 380°C is necessary to initiate the reaction because of CNF high graphitization degree[45]. Only POE binder was then fluorinated and EDX analysis indicated F/C value of 0.1. EDX spectrum and cartography are shown in supplementary information (Fig. SI2).

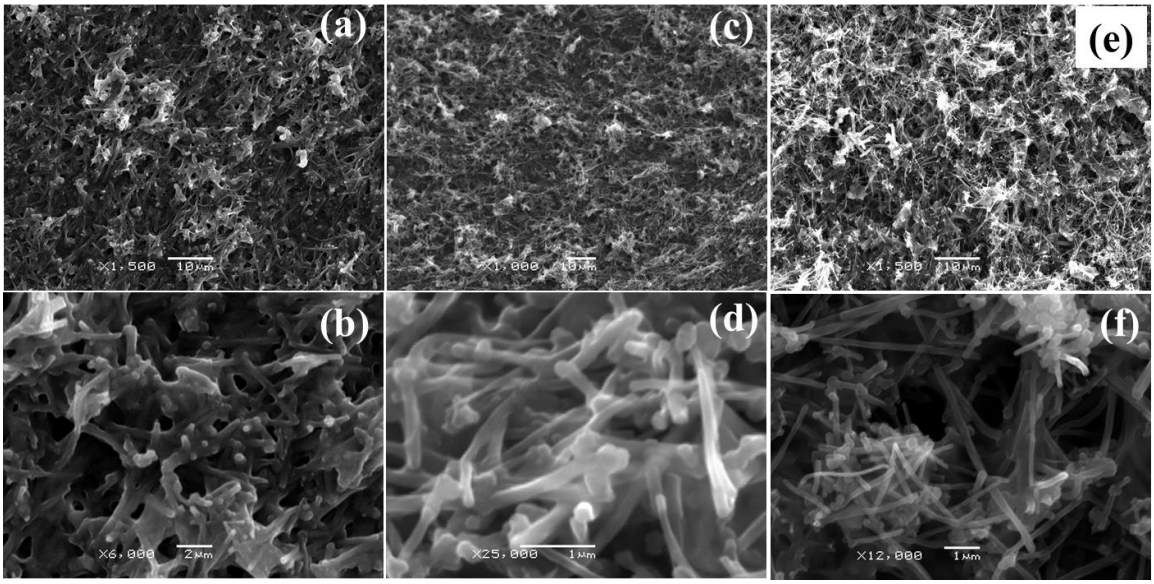

Figure 4. SEM images of F-CNF/PVDF (a, b), CNF/POE nanocomposite (c,d) and CNF/POE fluorinated with 50 mbar pressure of F_2 for 30 min (e,f) (40 w. % of F-CNF or CNF).

By covalent grafting of fluorine atoms onto POE surface the contact angle increased to 153 ± 2°. A significant increase from 80 ± 2° to 153 ± 2° was then achieved thanks to the presence of fluorinated layer onto the outmost surface of POE. The fluorinated POE probably covers the whole surface of the fibers to reach superhydrophobicity. The percentage of the polymer binder (40 w.%), PVDF and POE, seems to be efficient to totally cover the nanofibers and impose its surface chemistry.

The contact angle of F-CNF/PVDF strongly depends on the preparation route, dip coating or drop casting (Table 3). After this latter process, the value was of 142 ± 2°. The control of the texturing remains difficult at the microscale. Micro-texturing of F-CNF/PVDF nanocomposite film was then performed by ablation with a femtosecond laser. Among the huge range of shapes

and geometries that could be designed, a slot width of 40 µm and a pitch of 60 µm was selected according to the Cassie-Baxter model applied to parallelepiped slots. The theoretical contact angle for such a geometry is around 160°.

A representative example of film micro-structuring made with fluorinated nanofibers into a PVDF matrix is shown in figure 5. A second structuring at the nanometric scale is added by the emergence of nanofibers due to partial polymer decomposition by energy dissipation in the surrounding irradiated regions. The experimental contact angle was of 157 ± 2° in good accordance with theoretical value (160°). The obtained surface texturing of F-CNF/PVDF films favored the trapping of air cushions beneath the water drop, leading to the so-called Cassie state. This latter competed with the Wenzel (impaled) state where the liquid fully wetted the substrate. The value of 157 ± 2° remained unchanged for several weeks in accordance with the inertness of both the fluorinated nanofibers and PVDF and with the PVDF's efficiency to bind the nanofibers.

The third route used the same concept, however a conventional commercial polymer (polystyrene) was added onto the fluorinated nanofibers by an original method: fluorination of the fibers followed by the monomer gaseous phase grafting (Figure 1).

Table 3: F-CNF/PVDF nanocomposite and PVDF films water contact angle.

Film	PVDF	F-CNF/PVDF 40 w. % (dip coating)	F-CNF/PVDF 40 w. % (drop casting)	CNF/POE 40w.%	Fluorinated CNF/POE 40w.%
Contact angle	110± 2°	133± 2°	142 ± 2°	80 ± 2°	153 ± 2°

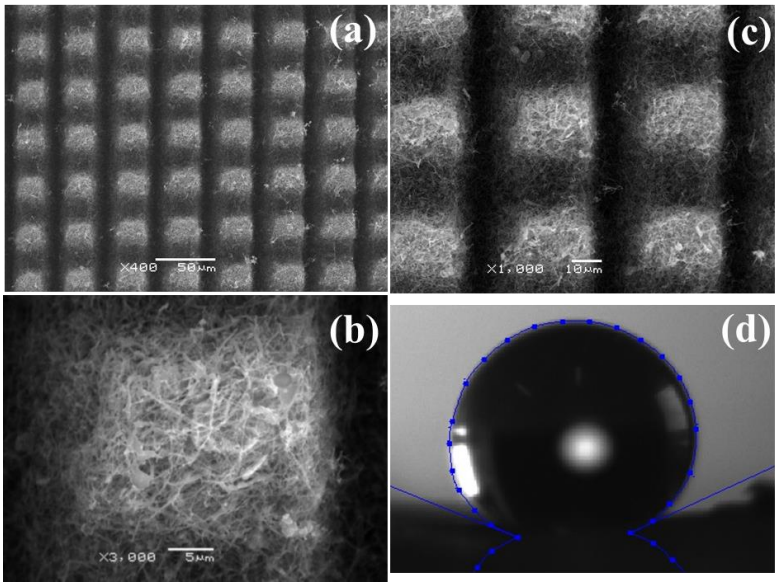

Figure 5. SEM images of F-CNF/PVDF micro-structured by ablation with femtosecond laser (a, b,c) and corresponding contact angle (d).

3.3 Route 3

The CNF fluorination ratio was estimated by weight uptake as $CF_{0.26\pm0.04}$ in good accordance with NMR data ($CF_{0.21\pm0.02}$) [48]. The chemical composition after grafting was also estimated by weight uptake as $CF_{0.21}(C_8H_8)_{0.67}$. Multi-nuclei solid state NMR has definitely proven the grafting using both ^{13}C, ^{19}F and ^{1}H MAS and $^{1}H \rightarrow ^{13}C$ cross-polarization CP-MAS experiments as it is shown below. The FCNF-PS after toluene evaporation SEM images (Fig. 6) underlined interspersed grafted and fluorinated nanofibers homogeneous dispersion. Continuous polystyrene matrix acted as a binder, see Figure 6c and d. Numerous fluorinated nanofibers emerged from the surface.

The water contact angle was of 156° ± 3° and remained unchanged for several weeks. The surface texturing was also efficient in this case as for F-CNF/PVDF film. The FCNF-PS film surface texture was stabilized because of two reasons: i) the nanofibers were strongly embedded into the PS matrix; grafting of styrene monomer occurred onto the carbonaceous surface and the polymer grew starting from this surface and ii) the surface chemistry was invariant with time and the polymer was covalently grafted onto the carbonaceous surface. Moreover, the C-F bonds covalence provided high thermal and chemical stability (heating at temperature higher than 350°C was necessary to remove the fluorine atoms).

Contact angle of PS flat film was equal to 87 ± 2°. The PS film direct fluorination with 50/50 vol.% F_2/N_2 flux at room temperature resulted in a decrease of this angle to 72 and 69 ± 2° when the duration was 5 and 60 min, respectively. FTIR was used to check fluorination efficiency. Fig. SI3 in supplementary information displays FTIR spectra recorded using ATR mode. Only the upper surface was analyzed with such way. Vibration modes of –CF– groups (–CHF–, $–CF_2–$, $–CF_3$) between 1300 and 800 cm^{-1} were observed. The overlapping of those bands results in the observed broad band. Surface tended to become more hydrophilic after fluorination regardless of the treatment condition. Several reasons can be developed to explain this modification. First, the polar component has been increased due to a formation of specific polar groups such as –FC=O and CHF and (C=O)OH, formed due to –FC=O groups hydrolysis ($-FC=O+H_2O \rightarrow -(C=O)OH + HF$) on the polymer surface in dynamic conditions (50/50 vol.% F_2/N_2 flux).

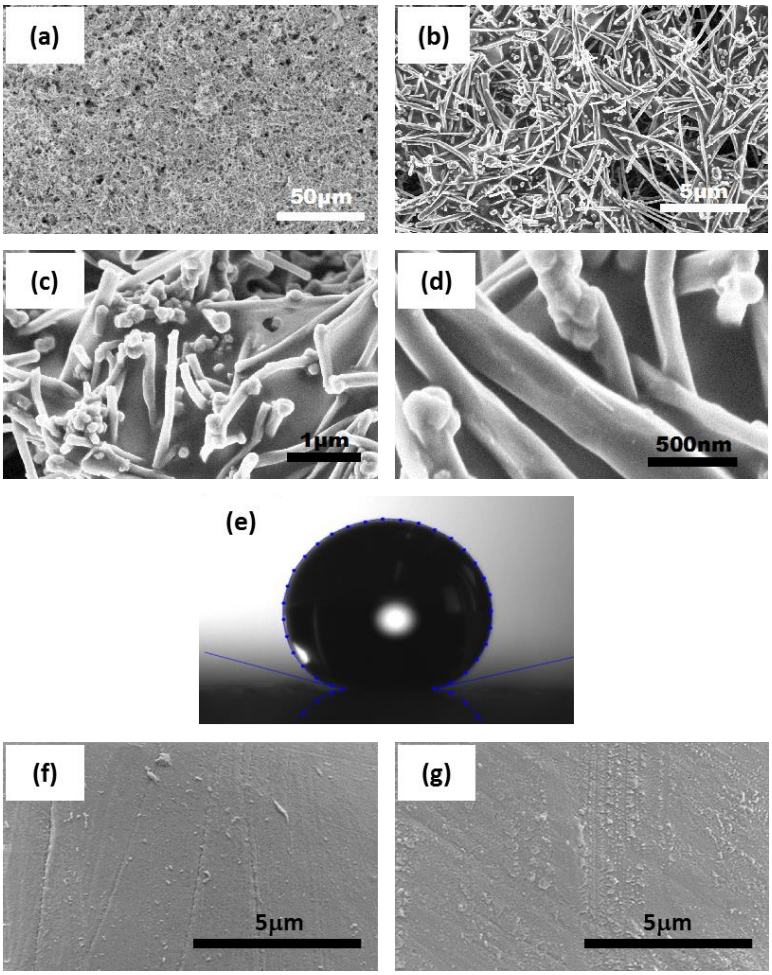

Figure 6. FCNF-PS films SEM images (a to d) and water contact angle (e); SEM images of flat PS film (f) and fluorinated PS film (g).

Oxygen played also a key role in this increase; several oxygen sources could be involved either during the process or after the reaction during the exposure to air. Some C-H and C-C bonds could be broken during the fluorination processes, forming dangling bonds (radicals), which reacted with oxygen and moisture from air.

SEM images of fluorinated flat PS film revealed that the roughness was increased after fluorination. Nevertheless, the roughness is not as important as for the case of FCNF-PS film. Once again, both presence of fluorine atoms and micro/nano-texturing are important parameters to consider in order to reach superhydrophobic properties.

4. DISCUSSION : HOW FLUORINE ATOMS ACT

For the two first routes, the presence of fluorine atoms allows an increase of the hydrophobic character. This shift is not enough to convert by fluorination the surface of flat resin in route 1. Micro-texturing of the resin with the present geometry does not avoid the filling of the gap by water because of the high hydrophilicity of the resin. The slight shift of hydrophobicitydue to the fluorination, denoted δH_F, allows a metastable state to be obtained: air is still trapped in the gap of the microstructure and the

behaviour turns to highly hydrophobic (i.e. Cassie-Baxter state). Our aim was not to optimize the micro-texturing but to evidence the role of the fluorine atoms (see figure 7). In the second route, F atoms can be added in a nanocomposite either in the polymer matrix or onto the fillers. Once again the nano-texturing is fixed because it results from the emergence of the nanofibers with diameter of around 150-180 nm (only use of fillers with different shape or size may change the nanostructure). The diameter distribution of raw fibers is quite narrow, included between 80 and 350 nm. The average diameter (<Φ>) is estimated to be near 150 nm from TEM and SEM observations of various parts of the raw sample. Because of the accommodation of the fluorine atoms within the graphene layers, fluorination results in an increase in the average diameter after fluorination (<Φ> = 180 nm) [63]. Experiment with POE underlines that the polymer imposes the intrinsic surface energy of the composite. With a given nano-texturing, δH_F is also added by the fluorination of POE allowing the superhydrophobicity because of a Cassie-Baxter state. The same conclusion can be done for FCNF-PVDF composite, efficient F atoms being those of PVDF matrix. Nevertheless, contact angles are lower for FCNF-PVDF composites (133 and 142°) than for fluorinated CNF-POE (153°). For the case of FCNF-PVDF, additional micro-texturing is necessary to reach the Cassie-Baxter state; It was achieved by laser ablation. The difference could be assigned to the swelling of the fibers during fluorination. Nano-texturing consists in tips of 150 nm (average value) and 180 nm for raw and fluorinated fibers, respectively. The difference between drop casting and dip-coating may be explained by the thickness of polymer layer onto the fibers that also slightly changes the nano-texturing. Fluorinated nanofibers are covered with polystyrene in the third route, δH_F due to F atoms is then masked but the polymer is enough hydrophobic to increase the contact angle thank to the nano-texturing. It is to note for this case that the average diameter of fibers is close to 150 nm because of the low fluorine content (F/C =0.21).

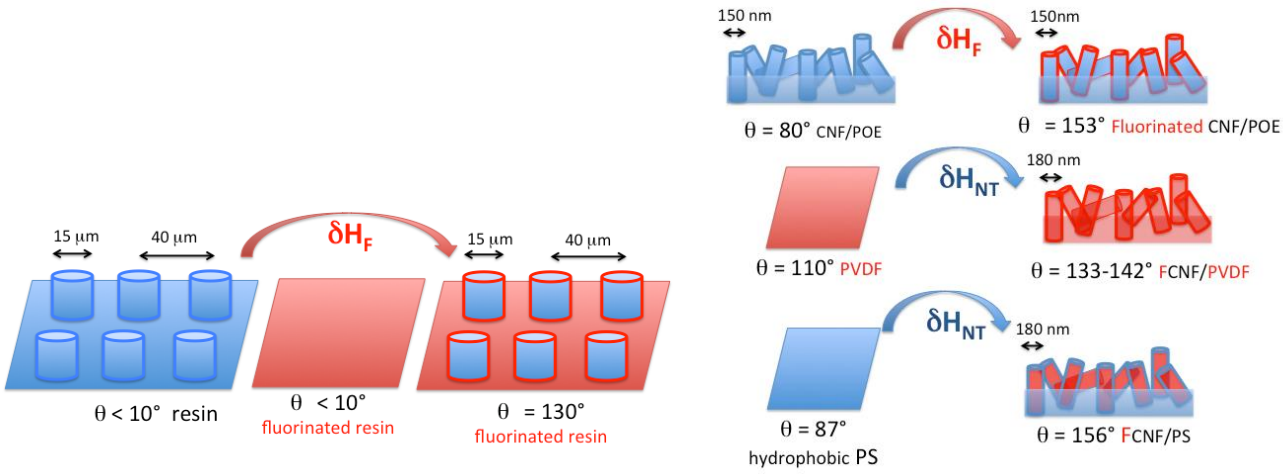

Figure 7. Schematic view of the increase in hydrophobicity due to the presence of fluorine atoms (δH_F) or nano-texturing (δH_{NT}). Red colour evidences the presence of fluorine.

5. CONCLUSION

Direct fluorination of polymers or carbonaceous materials was not very frequently used to reach superhydrophobicity. It could be explained by the difficulties in the control of the treatment conditions and in avoiding polymer decomposition, especially when the polymer was micro-textured. Because of the polymer lattice decomposition into CF_4 and C_2F_6 gaseous species in

fluorine atmosphere, the micro-texturing might be lost. Use of atomic fluorine F• released during the decomposition of a fluorinating agent such as XeF_2 overcame those difficulties and allowed for the polymer surface micro-texturing to be preserved. Both presence of fluorine atoms on the polymer surface and micro-texturing were necessary to convert the surface from hydrophilic (water contact angle θc <10°) to hydrophobic one (θc =131±2 °) but not sufficient to obtain superhydrophobic properties. Surface micro/nano-texturing could be formed by the emergence of the fillers from the nanocomposite bulk. On the other hand, the presence of the fluorine atoms was achieved by the carbon nanofibers direct fluorination (treatment with gaseous F_2). Fluorinated polymer such as PDVF as well as commercial hydrophobic polymers like polystyrene could act as binders and/or polymer matrices that stabilize the nanocomposite. Polystyrene was covalently grafted onto the nanofiber surface through a two-step process: fluorination followed by a monomer grafting. The polymerization of styrene ensured both covalent grafting onto the carbonaceous surface and a good dispersion of nanofibers inside the polymer matrix. Moreover, the C-F bonds exhibited covalent nature in fluorinated nanofibers, in PVDF, in fluorinated POE and in the fluorinated resin, and ensured improved chemical stability to the studied nanocomposites and micro-textured resin. The measured water contact angles of 131, 134, 153 and 156° for fluorinated micro-textured resin, F-CNF/PVDF, fluorinated CNF/POE and FCNF-PS nanocomposites, respectively, were not changed with time. For F-CNF/PVDF, an additional step of micro-texturing by femtosecond laser ablation was necessary to reach the superhydrophobity and a contact angle of 157°. Comparison of the water contact angles for nanocomposites with PVDF, POE and fluorinated POE highlights that the polymer matrix imposes its surface chemistry whereas the emergence of nanofibers results in nano-texturing.

Acknowledgements

The research was partially (concerning the ”Route 3” results) funded by the grant of the Russian Scientific Foundation (project 15-13-10038).

References

[1] L. Yao, J. He, Recent progress in antireflection and self-cleaning technology – From surface engineering to functional surfaces, *Prog. Mater. Sci.*, 61 (2014) 94-143.
[2] B. Bhushan, Y.C. Jung, Natural and biomimetic artificial surfaces for superhydrophobicity, self-cleaning, low adhesion, and drag reduction, *Prog. Mater. Sci.*, 56 (2011) 1-108.
[3] A.M. Mohamed, A.M. Abdullah, N.A. Younan, Corrosion behavior of superhydrophobic surfaces: A review, *Arabian J. Chem.*, 8 (2015) 749-765.
[4] Q. Xie, J. Xu, L. Feng, L. Jiang, W. Tang, X. Luo, C.C. Han, Facile Creation of a Super-Amphiphobic Coating Surface with Bionic Microstructure, *Adv. Mater.*, 16 (2004) 302-305.
[5] T. Sun, H. Tan, D. Han, Q. Fu, L. Jiang, No platelet can adhere--largely improved blood compatibility on nanostructured superhydrophobic surfaces, *Small*, 1 (2005) 959-963.
[6] R.N. Wenzel, Resistance of solid surfaces to wetting by water, *Ind. Eng. Chem.*, 28 (1936) 988-994.

[7] A. Cassie, S. Baxter, Wettability of porous surfaces, *Trans. Faraday Soc.*, 40 (1944) 546-551.
[8] H. Ogihara, J. Xie, T. Saji, Factors determining wettability of superhydrophobic paper prepared by spraying nanoparticle suspensions, *Colloid Surface A*, 434 (2013) 35-41.
[9] T. Sun, L. Feng, X. Gao, L. Jiang, Bioinspired surfaces with special wettability, *Acc. Chem. Res.*, 38 (2005) 644-652.
[10] D. Bechert, M. Bruse, W. Hage, Experiments with three-dimensional riblets as an idealized model of shark skin, *Exp. Fluids*, 28 (2000) 403-412.
[11] X. Gao, L. Jiang, Biophysics: water-repellent legs of water striders, *Nature*, 432 (2004) 36.
[12 M. Cao, X. Song, J. Zhai, J. Wang, Y. Wang, Fabrication of highly antireflective silicon surfaces with superhydrophobicity, *J. Phys. Chem. B*, 110 (2006) 13072-13075.
[13] T. Ishizaki, M. Sakamoto, Facile formation of biomimetic color-tuned superhydrophobic magnesium alloy with corrosion resistance, *Langmuir*, 27 (2011) 2375-2381.
[14] J. Liang, Y. Hu, Y. Wu, H. Chen, Fabrication and Corrosion Resistance of Superhydrophobic Hydroxide Zinc Carbonate Film on Aluminum Substrates, *J. Nanomaterials*, 2013 (2013) 1-6.
[15] Y. Hu, S. Huang, S. Liu, W. Pan, A corrosion-resistance superhydrophobic TiO2 film, *Appl. Surf. Sci.*, 258 (2012) 7460-7464.
[16] J. Song, W. Xu, Y. Lu, X. Liu, Z. Wei, J. Sun, Fabrication of superhydrophobic surfaces with hierarchical rough structures on Mg alloy substrates via chemical corrosion method, *Micro & Nano Lett.*, IET, 7 (2012) 204-207.
[17] E.T. de Givenchy, S. Amigoni, C. Martin, G. Andrada, L. Caillier, S. Geribaldi, F. Guittard, Fabrication of superhydrophobic PDMS surfaces by combining acidic treatment and perfluorinated monolayers, *Langmuir*, 25 (2009) 6448-6453.
[18] Y. Li, X.J. Huang, S.H. Heo, C.C. Li, Y.K. Choi, W.P. Cai, S.O. Cho, Superhydrophobic bionic surfaces with hierarchical microsphere/SWCNT composite arrays, *Langmuir*, 23 (2007) 2169-2174.
[19] E. Wohlfart, J.P. Fernández-Blázquez, E. Arzt, A. del Campo, Nanofibrillar Patterns on PET: The Influence of Plasma Parameters in Surface Morphology, *Plasma Process. Polym.*, 8 (2011) 876-884.
[20] J.D. Brassard, D.K. Sarkar, J. Perron, Synthesis of monodisperse fluorinated silica nanoparticles and their superhydrophobic thin films, *ACS Appl. Mater. Interfaces*, 3 (2011) 3583-3588.
[21] D. Zhu, X. Lu, Q. Lu, Electrically conductive PEDOT coating with self-healing superhydrophobicity, *Langmuir*, 30 (2014) 4671-4677.
[22] Y. Chong, N. Watanabe, A novel composite having superhydrophobic properties, J. Fluorine Chem. 54 (1991) 43.
[23] M.M. T. Nishino, M. Meguro, K. Nakamae, M.Matsushita, Y. Ueda, The lowest surface free energy based on -CF3 alignment, *Langmuir*, 15 (1999) 4321-4323.
[24] A. Tropmann, L. Tanguy, P. Koltay, R. Zengerle, L. Riegger, Completely superhydrophobic PDMS surfaces for microfluidics, *Langmuir*, 28 (2012) 8292-8295.
[25] B. Bhushan, Y.C. Jung, Micro- and nanoscale characterization of hydrophobic and hydrophilic leaf surfaces, *Nanotechnology*, 17 (2006) 2758-2772.
[26] Y.C. Jung, B. Bhushan, Contact angle, adhesion and friction properties of micro-and nanopatterned polymers for superhydrophobicity, *Nanotechnology*, 17 (2006) 4970-4980.
[27] R.D. Mundo, F. Palumbo, R. d'Agostino, Nanotexturing of polystyrene surface in fluorocarbon plasmas: from sticky to slippery superhydrophobicity, *Langmuir*, 24 (2008) 5044-5051.
[28] J. Fresnais, J.P. Chapel, F. Poncin-Epaillard, Synthesis of parent superhydrophobic polyethylene surfaces, *Surf. Coat. Technol.*, 200 (2006) 5296-5305.
[29] M. Manca, B. Cortese, I. Viola, A.S. Aricò, R. Cingolani, G. Gigli, Influence of chemistry and topology effects on superhydrophobic CF4-plasma-treated poly (dimethylsiloxane)(PDMS), *Langmuir*, 24 (2008) 1833-1843.
[30] B. Cortese, S. D'Amone, M. Manca, I. Viola, R. Cingolani, G. Gigli, Superhydrophobicity due to the hierarchical scale roughness of PDMS surfaces, *Langmuir*, 24 (2008) 2712-2718.
[31] P.S. Brown, E.L. Talbot, T.J. Wood, C.D. Bain, J.P. Badyal, Superhydrophobic hierarchical honeycomb surfaces, *Langmuir*, 28 (2012) 13712-13719.
[32] E. Jeong, T.-S. Bae, S.-M. Yun, S.-W. Woo, Y.-S. Lee, Surface characteristics of low-density polyethylene films modified by oxyfluorination-assisted graft polymerization, *Colloids and Surfaces A: Physicochemical and Engineering Aspects*, 373 (2011) 36-41.
[33] W. Jiang, C.M. Grozea, Z. Shi, G. Liu, Fluorinated raspberry-like polymer particles for superamphiphobic coatings, *ACS Appl. Mater. Interfaces*, 6 (2014) 2629-2638.
[34] T. Darmanin, F. Guittard, Molecular design of conductive plymers to modulate superoleophobic properties, J.A.C.S., 131 (2009) 7928-7933.
[35] T. Darmanin, E. Taffin de Givenchy, S. Amigoni, F. Guittard, Superhydrophobic surfaces by electrochemical processes, *Adv. Mater*, 25 (2013) 1378-1394.

[36] A. Tuteja, W. Choi, M. Ma, J.M. Mabry, S.A. Mazzella, G.C. Rutledge, G.H. McKinley, R.E. Cohen, Designing superoleophobic surfaces, *Science*, 318 (2007) 1618-1622.
[37] R.T. Rajendra Kumar, K.B. Mogensen, P. Bøggild, Simple approach to superamphiphobic overhanging silicon nanostructures, *J. Phys. Chem. C*, 114 (2010) 2936-2940.
[38] J.-Y. Shiu, C.-W. Kuo, P. Chen, C.-Y. Mou, Fabrication of tunable superhydrophobic surfaces by nanosphere lithography, *Chem. Mater.*, 16 (2004) 561-564.
[39] S. Coulson, I. Woodward, J. Badyal, S. Brewer, C. Willis, Super-repellent composite fluoropolymer surfaces, *J. Phys. Chem. B*, 104 (2000) 8836-8840.
[40] M. Toma, G. Loget, R.M. Corn, Flexible Teflon nanocone array surfaces with tunable superhydrophobicity for self-cleaning and aqueous droplet patterning, *ACS Appl. Mater. Interfaces*, 6 (2014) 11110-11117.
[41] H. Sawada, T. Suzuki, H. Takashima, Preparation and properties of fluoroalkyl end-capped vinyltrimethoxysilane oligomeric nanoparticles – A new approach to facile creation of a completely superhydrophobic coating surface with these nanoparticles. Colloid Polym. Sci. 286 (2008) 1569–1574.
[42] C.-T. Hsieh, W.-Y. Chen, F.-L. Wu, Fabrication and superhydrophobicity of fluorinated carbon fabrics with micro/nanoscaled two-tier roughness, *Carbon*, 46 (2008) 1218-1224.
[43] L.Y. Meng, S.J. Park, Effect of fluorination of carbon nanotubes on superhydrophobic properties of fluoro-based films, *J. Colloid Interface Sci.*, 342 (2010) 559-563.
[44] H. Kinoshita, A. Ogasahara, Y. Fukuda, N. Ohmae, Superhydrophobic/superhydrophilic micropatterning on a carbon nanotube film using a laser plasma-type hyperthermal atom beam facility, *Carbon*, 48 (2010) 4403-4408.
[45] M. Sansotera, W. Navarrini, G. Resnati, P. Metrangolo, A. Famulari, C.L. Bianchi, P.A. Guarda, Preparation and characterization of superhydrophobic conductive fluorinated carbon blacks, *Carbon*, 48 (2010) 4382-4390.
[46] L. Wang, Y. Zhao, K. Lin, X. Zhao, Z. Shan, Y. Di, Z. Sun, X. Cao, Y. Zou, D. Jiang, Super-hydrophobic ordered mesoporous carbon monolith, *Carbon*, 44 (2006) 1336-1339.
[47] A. Kharitonov, G. Simbirtseva, A. Tkachev, A. Blohin, T. Dyachkova, A. Maksimkin, D. Chukov, Reinforcement of epoxy resin composites with fluorinated carbon nanotubes, *Comp. Sci. Technol.*, 107 **(**2015) 162-168.
[48] A. Kharitonov, J. Zha, M. Dubois, Tunable hydrophylicity/hydrophobicity of fluorinated carbon nanotubes via graft polymerization of gaseous monomers, *J. Fluorine Chem.*, 178 (2015) 279-285.
[49] J.G. Malm, H. Selig, J. Jortner, S.A. Rice, The chemistry of xenon, *Chem. Rev.*, 65 (1965) 199-236.
[50] J. Zha, N. Batisse, D. Claves, M. Dubois, L. Frezet, A. P. Kharitonov, L. N. Alekseiko, Superhydrophocity via gas-phase monomers grafting onto carbon nanotubes,*Progr. Surf. Sci.*, 91 (2016) 57-71.
[51] D.A. Shirley, High-resolution X-ray photoemission spectrum of the valence bands of gold, Phys. Rev. B, 972, 5, 4709.
[52] J.H. Scofield, Hartree-Slater subshell photoionization cross-sections at 1254 and 1487 eV, *J. Electron Spectrosc. Relat. Phenom.*, 8 (1976) 129-137.
[53] S. Tanuma, C.J. Powell, D.R. Penn, Calculations of electron inelastic mean free paths for 31 materials, *Surf. Interface Analysis*, 11 (1988) 577-589.
[54] V. Nazarov, Structure and composition of the surface layer in polymers modified by elemental fluorine, *J. Appl. Polym. Sci.*, 95 (2005) 897-902.
[55] G. Nansé, E. Papirer, P. Fioux, F. Moguet, A. Tressaud, Fluorination of carbon blacks: an X-ray photoelectron spectroscopy study: III. Fluorination of different carbon blacks with gaseous fluorine at temperatures below 100 C influence of the morphology, structure and physico-chemical characteristics of the carbon black on the fluorine fixation, *Carbon*, 35 (1997) 515-528.
[56] G. Nanse, E. Papirer, P. Fioux, F. Moguet, A. Tressaud, Fluorination of carbon blacks. An X-ray photoelectron spectroscopy study. Part II. XPS study of a furnace carbon black treated with gaseous fluorine at temperatures below 100 C. Influence of the reaction parameters and of the activation of the carbon black on the fluorine fixation, *Carbon*, 35 (1997) 371-388.
[57] G. Socrates, Infrared and Raman characteristic group frequencies: tables and charts, *John Wiley & Sons*, 2004.
[58] A. Panich, Nuclear magnetic resonance study of fluorine–graphite intercalation compounds and graphite fluorides, *Synth. Met.*, 100 (1999) 169-185.
[59] H. Touhara, F. Okino, Property control of carbon materials by fluorination, *Carbon*, 38 (2000) 241-267.
[60] T. Mallouk, B. Hawkins, M. Conrad, K. Zilm, G. Maciel, N. Bartlett, Raman, Infrared and nmr Studies of the Graphite Hydrofluorides), *Philo. Trans. R. S. London Ser. A.*, 314 (1985) 179-187.
[51] W. Zhang, P. Bonnet, M. Dubois, C.P. Ewels, K. Guérin, E. Petit, J.-Y. Mevellec, L. Vidal, D.A. Ivanov, A. Hamwi, Comparative study of SWCNT fluorination by atomic and molecular fluorine, *Chem. Mater.*, 24 (2012) 1744-1751.
[62] A. Tressaud, F. Moguet, S. Flandrois, M. Chambon, C. Guimon, G. Nanse, E. Papirer, V. Gupta, and O.P. Bahl. *J. Phys. Chem. Solids*, 57 (1996) 745.

[63] W. Zhang, K. Guérin, M. Dubois, Z. Fawal, D. Ivanov, L. Vidal, A. Hamwi, Carbon nanofibres fluorinated using TbF4 as fluorinating agent Part I: Structural properties", Carbon 46 (2008) 1010- 1016.